

# Local Abundance of Macular Xanthophyll Pigment Is Associated with Rod- and Cone-Mediated Vision in Aging and Age-Related Macular Degeneration

Deepayan Kar,<sup>1</sup> Mark E. Clark,<sup>1</sup> Thomas A. Swain,<sup>1,2</sup> Gerald McGwin Jr.,<sup>1,2</sup> Jason N. Crosson,<sup>1,3</sup> Cynthia Owsley,<sup>1</sup> Kenneth R. Sloan,<sup>1,4</sup> and Christine A. Curcio<sup>1</sup>

<sup>1</sup>Department of Ophthalmology and Visual Sciences, School of Medicine, University of Alabama at Birmingham, Birmingham, Alabama, United States

<sup>2</sup>Department of Epidemiology, School of Public Health, University of Alabama at Birmingham, Birmingham, Alabama, United States

<sup>3</sup>Retina Consultants of Alabama, Birmingham, Alabama, United States

<sup>4</sup>Department of Computer Science, School of Arts and Sciences, University of Alabama at Birmingham, Birmingham, Alabama, United States

Correspondence: Christine A. Curcio, Department of Ophthalmology and Visual Sciences, EyeSight Foundation of Alabama Vision Research Laboratories, School of Medicine, University of Alabama at Birmingham, 1670 University Boulevard, Room 360, Birmingham, AL 35294-0099, USA; [christinecurcio@uabmc.edu](mailto:christinecurcio@uabmc.edu).

Received: May 8, 2020

Accepted: June 25, 2020

Published: July 30, 2020

Citation: Kar D, Clark ME, Swain TA, et al. Local abundance of macular xanthophyll pigment is associated with rod- and cone-mediated vision in aging and age-related macular degeneration. *Invest Ophthalmol Vis Sci.* 2020;61(8):46. <https://doi.org/10.1167/iovs.61.8.46>

**PURPOSE.** We assessed the association between the abundance of macular xanthophyll carotenoid pigment using dual-wavelength autofluorescence and multimodal vision testing including rod-mediated dark adaptation (RMDA), a measure of retinoid re-supply, in adults  $\geq 60$  years old with and without age-related macular degeneration (AMD).

**METHODS.** AMD severity was determined using the nine-step Age-Related Eye Disease Study grading. Tests probed cones (best-corrected visual acuity, contrast sensitivity), cones and rods (low-luminance visual acuity, low-luminance deficit, mesopic light sensitivity), or rods only (scotopic light sensitivity, RMDA). Signal attenuation by macular pigment optical density (MPOD) was estimated using a ratio of blue and green autofluorescence signal to yield mean MPOD in a 1°-diameter fovea-centered disk, mean MPOD in a 2°-diameter disk centered on a perifoveal RMDA test location, and macular pigment optical volume (MPOV, or integrated MPOD) in a 4°-diameter fovea-centered disk. Age-adjusted associations between vision and imaging measures were determined.

**RESULTS.** In 88 eyes of 88 subjects (age,  $74.9 \pm 5.8$  years) with normal eyes ( $n = 32$ ), early AMD ( $n = 23$ ), or intermediate AMD ( $n = 33$ ), foveal and perifoveal MPOD and MPOV were higher in the AMD eyes than in the normal eyes. At the RMDA test location, higher MPOD was unrelated to AMD severity but was associated with faster RMDA.

**CONCLUSIONS.** In older adults with and without AMD, higher macular xanthophyll concentrations are associated with better best-corrected visual acuity and RMDA. Data are consistent with a model of cone resilience and rod vulnerability in aging and AMD and can be further explored in a larger sample study.

Keywords: autofluorescence, macular xanthophyll pigment, Müller glia, rod-mediated dark adaptation, cone-mediated vision, age-related macular degeneration, fundus grading

Age-related macular degeneration (AMD) causes vision loss globally<sup>1</sup> and involves dysfunction of the choriocapillary endothelium, retinal pigment epithelium (RPE), and photoreceptors, with reactive gliosis, in the setting of extracellular deposits between the outer retina and circulation. The macular pigment (MP) is comprised of two xanthophyll carotenoids of dietary origin—(3R,3'R,6'R)-lutein and (3R,3'R)-zeaxanthin—and a metabolite, (3R,3'S;meso)-zeaxanthin.<sup>2</sup> Oral supplements containing lutein, zeaxanthin, and vitamins are recommended for some patients with non-neovascular AMD.<sup>3</sup> Hypothesized beneficial properties of MP include antioxidant protection,<sup>4</sup> improved visual performance and comfort via short wavelength light-filtering and dichroism,<sup>5,6</sup> and direct interaction with neurons.<sup>7</sup> Xanthophylls are also detected in brain.<sup>8,9</sup> Greater insight

into MP biology and role in vision is possible now, due to progress in AMD pathophysiology and imaging.

A proposal that Müller glia are major xanthophyll reservoirs<sup>10</sup> is gaining traction,<sup>11</sup> supported by recent research on glio-degenerative disease<sup>12-17</sup> and evidence in the available localization studies. Yellow MP is highly concentrated in the foveal center and extends radially outward in the Henle fiber, inner plexiform, and nerve fiber layer. This pattern, first seen with microdensitometry (Fig. 1),<sup>18,19</sup> was recently replicated and extended with Raman resonance microscopy to show high zeaxanthin centrally.<sup>20</sup> The distribution includes cones, as originally described,<sup>21</sup> as well as rods and Müller glia outer trunks in the Henle fiber layer<sup>22,23</sup> and lateral glial extensions in the other layers. Xanthophyll concentration characteristically falls off sharply with distance from

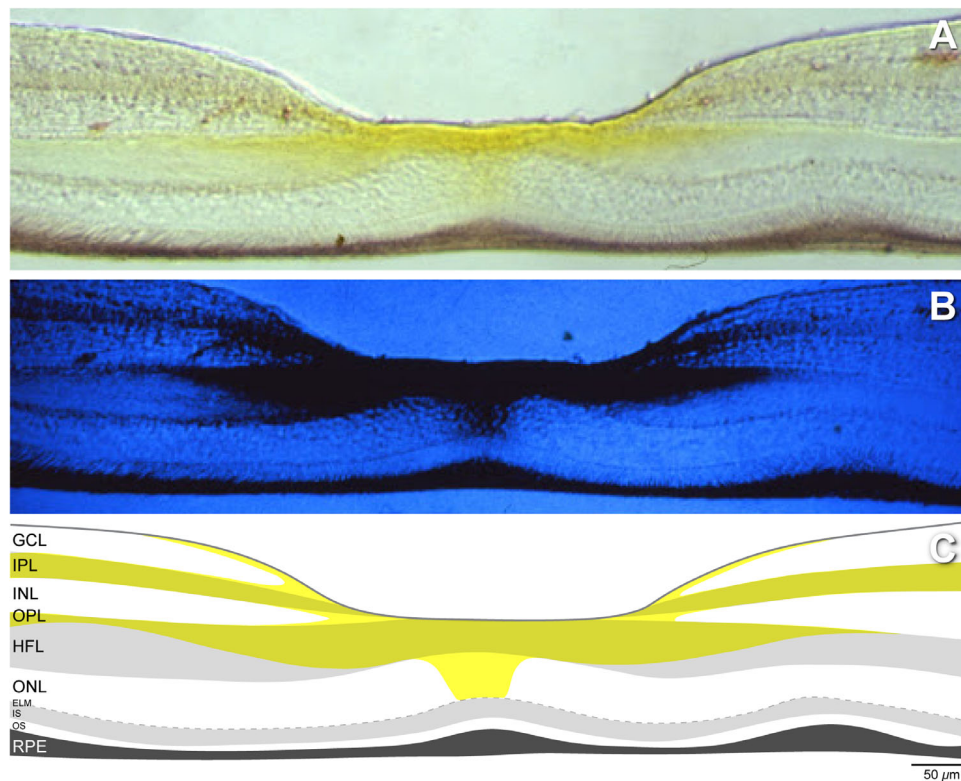


**FIGURE 1.** Retinal distribution of xanthophyll carotenoid pigment. **(A)** Vertical frozen histological section through the fovea of a rhesus monkey retina imaged with dual-wavelength microdensitometry. **(B)** Yellow xanthophyll pigment absorbs short-wavelength blue light and hence appears dark. **(C)** Schematic of the laminar distribution of the macular xanthophyll pigment, drawn anew from the images in the top and middle panels. Xanthophyll pigment is concentrated at the foveal center, the Henle fiber, inner plexiform, and nerve fiber layers. Images in **A** and **B** were downloaded from the website of Max Snodderly, PhD (<http://www.sbs.utexas.edu/SnodderlyLab/gallery.html>). The images were originally published in monochrome.<sup>18</sup>

the foveal center. Individual variation manifesting as central peaks, rings, and plateaus is related to variation in foveal structure seen in optical coherence tomography (OCT).<sup>11</sup>

Xanthophyll concentration in the retinal projection plane, referred to as macular pigment optical density (MPOD), is commonly estimated using heterochromatic flicker photometry (HFP), a psychophysical color-matching technique. Past research with HFP has shown that better cone-mediated vision, including acuity and contrast sensitivity, is associated with higher MPOD levels in cross-sectional studies of younger adults.<sup>24–26</sup> In older normal adults, MPOD is associated with better light sensitivity.<sup>27</sup> Most studies<sup>6,25,26,28–31</sup> (but not all<sup>32</sup>) of normal eyes of persons consuming dietary supplements with xanthophyll report improved photopic and mesopic vision. For both younger and older normal eyes, greater MPOD assessed by HFP was linked to better scotopic and mesopic sensitivity and mesopic visual acuity.<sup>5,27,33</sup> A small sample report related slowed rod-mediated dark adaptation (RMDA) in older adults to higher foveal MPOD.<sup>35</sup> However, in a large sample of older adults with normal maculas ( $N = 306$ ), we could not confirm this finding.<sup>34</sup>

Drawbacks of HFP for estimating MPOD include difficulty for some older patients and the limited number of retinal locations tested. MPOD can now be assessed with dual-wavelength autofluorescence imaging, based on emission signals elicited from the RPE by blue and green excita-

tion lights. Intensities at fixation, where blue light is blocked by MP, are compared to intensities at an eccentric reference point where MPOD is near zero, due to pigment drop-off with eccentricity. MPOD integrated over the central area, referred to as macular pigment optical volume (MPOV), is proposed as a comprehensive metric.<sup>35,36</sup> Relative to HFP, dual-wavelength autofluorescence MPOD imaging is quicker and more objective, repeatable, and unbiased (i.e., all pixels are included). Its interpretation can benefit from new data on the cellular and subcellular basis of RPE autofluorescence imaging.<sup>37–40</sup>

In persons  $\geq 60$  years of age with early or intermediate AMD or with normal maculas, we tested whether MP assessed using dual-wavelength autofluorescence is associated with aspects of cone- and rod-mediated vision, including RMDA. In this exploratory study, we found that higher foveal MPOD was associated with better cone-mediated acuity, greater retinal thickness, and AMD severity and that higher MPOD at the RMDA test location was associated with better RMDA across severity groups.

## METHODS

The study followed the tenets of the Declaration of Helsinki and was approved by the Institutional Review Board at the University of Alabama at Birmingham (UAB). Study

participants provided written informed consent after the nature and purpose of the study were described.

Participants were recruited from the comprehensive eye care and retina clinics in the Callahan Eye Hospital at UAB. One eye of each participant meeting criteria for normal macular health, early AMD, or intermediate AMD was enrolled; when both eyes met entry criteria, the eye with better acuity was chosen to ensure that RMDA was measurable. Three-field digital stereo color fundus photographs (CFPs) (FF 450<sup>plus</sup>; Carl Zeiss Meditec, Dublin, CA, USA) were evaluated by an experienced grader (MEC) masked to other study variables (previously determined intra-observer agreement  $\kappa = 0.88$ , inter-observer agreement  $\kappa = 0.75$ <sup>41</sup>). Eyes receiving a step of 1 in the Age-Related Eye Disease Study (AREDS) nine-step classification system<sup>42,43</sup> were considered normal. There were 94 participants who completed dark adaptation testing and MPOD testing. Among those who completed these tests, those with central or non-central geographic atrophy or neovascularization ( $n = 6$ ) were excluded, resulting in a sample of  $N = 88$ . Study recruitment exclusion criteria included previous diagnoses of glaucoma, retina and optic nerve conditions, corneal disease, brain injury, diabetes, or neurological or psychiatric conditions as revealed by the medical record or self-report. Demographic and health-related characteristics (age, sex, race/ethnicity, oral carotenoid supplement use, smoking status) were obtained through participant interview. Lens status was determined from the medical record.

We acquired macular volumes with spectral-domain OCT (Spectralis HRA+OCT; Heidelberg Engineering, Heidelberg, Germany), where  $\lambda = 870$  nm, scan depth was 1.9 mm, axial resolution was 3.5  $\mu\text{m}$  per pixel in tissue, and lateral resolution was 14  $\mu\text{m}$  per pixel in tissue. B-scans ( $n = 73$ ) were horizontally oriented and centered over the fovea in a  $20^\circ \times 15^\circ$  ( $5.7 \times 4.2$ -mm) area. Automatic real-time averaging was 8 to 18, and quality (signal-to-noise) was 20 to 47 decibels (dB). Upon review of the OCT volumes, suspects for non-symptomatic type 1 neovascularization<sup>44,45</sup> were excluded, as described elsewhere.<sup>46</sup>

The Spectralis investigational MPOD module uses confocal scanning laser ophthalmoscopy with blue ( $\lambda = 488$  nm) and green ( $\lambda = 514$  nm) laser diodes for autofluorescence excitation. Initial camera alignment, illumination, and focus were done in near-infrared mode. The camera mode was switched to simultaneous 488 nm (blue) and 514 nm (green) imaging. Two movies of 140 frames over 30 seconds were captured by flickering the two excitation wavelengths, in combination with a barrier filter that blocks all wavelengths  $< 560$  nm. The Spectralis reports correction factors to accommodate for the fact that the excitation wavelengths are not identical to peak MP absorption ( $\sim 460$  nm).<sup>35</sup>

### Visual Function Testing

Functionally probed retinal regions are shown in Figure 2 in relation to an idealized distribution of MP. RMDA (Fig. 2A) was measured psychophysically (AdaptDx; MacuLogix, Harrisburg, PA, USA)<sup>47-49</sup> in one eye after dilation. The procedure began with a photo-bleach exposure to a flash (0.25-ms duration, 58,000 scotopic  $\text{cd}/\text{m}^2 \cdot \text{s}^{-1}$  intensity; equivalent  $\sim 83\%$  bleach) while the participant focused on the fixation light. The photo-bleach flash subtended  $6^\circ$  and was centered at  $5^\circ$  on the inferior vertical meridian (i.e., superior to the fovea on the retina), which was also the position of the test target. Threshold measurement for a  $2^\circ$ -

diameter circular target of 500-nm wavelength (green) light began 15 seconds after bleach offset, with participants pressing a button when a flashing target first became visible. Log thresholds were expressed as sensitivity in dB units as a function of time after bleach offset. Dark adaptation speed is defined by the rod intercept time,<sup>49</sup> the duration in minutes required for sensitivity to recover to a criterion value of  $5.0 \times 10^{-3}$  scotopic  $\text{cd}/\text{m}^2$ , in the latter half of the second component of RMDA.<sup>50,51</sup>

The eye tested for RMDA underwent additional vision tests, as follows. Best-corrected visual acuity (BCVA) was assessed via an electronic visual acuity (EVA) tester<sup>52</sup> (JAEB Center for Health Research, Tampa, FL, USA) under photopic conditions (Fig. 2D, expressed as logarithm of the minimum angle of resolution [logMAR]). Low-luminance visual acuity (Fig. 2D) was also assessed using the EVA with participants viewing letters through a 2.0-log unit neutral density filter to reduce luminance to 1  $\text{cd}/\text{m}^2$ .<sup>53</sup> Low-luminance deficit was defined by the increase in logMAR under mesopic conditions as compared to photopic conditions. Contrast sensitivity (Fig. 2C) was estimated by the Pelli-Robson chart<sup>54</sup> (Precision Vision, La Salle, IL, USA) under photopic conditions and scored by the letter-by-letter method.<sup>55</sup> Mesopic and scotopic sensitivity (Fig. 2B) was measured using the MP-1S microperimeter (Nidek Technologies, Padova, Italy), modified to increase the dynamic range of target light intensity to 30 dB.<sup>56,57</sup> Using a Goldmann III target ( $0.43^\circ$  diameter), sensitivity was measured at the fovea and four targets on each side of the fovea on the horizontal and vertical meridians, out to  $12^\circ$  eccentricity (17 total targets). For this study, sensitivity was expressed as an average of only the five most central test targets (Fig. 2B). Some participants did not have microperimetry testing, because the instrument was not available (74 completed this testing).

### Metrics for MPOD, MPOV, Rod:Cone Ratio, and Minimum Retinal Thickness

MPOD data was exported from the Spectralis and processed by custom FIJI plug-ins for ImageJ 1.52 (National Institutes of Health, Bethesda, MD, USA),<sup>58</sup> see Appendix for details. Exported data consisted of blue and green autofluorescence images and device-specific calibration parameters from the HEYEX software (Heidelberg Engineering) that was required for the wavelength correction mentioned above. As detailed elsewhere,<sup>36</sup> MPOD is the  $\log_{10}$  of the ratio of green-excited autofluorescence intensities to blue-excited autofluorescence intensities emitted by the RPE, calculated at each pixel location. From these two input images was produced a single MPOD image identical to the one displayed (but not exported) by the Spectralis. MPOD images were registered with the near-infrared reflectance Localizer images of the OCT volume, in which the location of the fovea had previously been marked manually in the associated B-scan stack.

Several custom FIJI plug-ins produced measurements similar to, but more customized than, the HEYEX MPOD analysis software. In particular, mean MPOD values were calculated for a central disk ( $1^\circ$  diameter,  $0^\circ$ - $0.5^\circ$  radius) and two annuli centered on the fovea, with inner and outer radii of  $0.5^\circ$  to  $2.0^\circ$  (parafovea) and  $2.0^\circ$ - $9.0^\circ$  (perifovea), respectively. We also computed the mean MPOV as  $\text{MPOD} \times \text{mm}^2$  for the disks with radii  $2.0^\circ$  and  $9.0^\circ$ . MPOD values were normalized by setting the mean MPOD value at eccentricity  $9.0^\circ$  to zero. The value of  $9.0^\circ$  is further

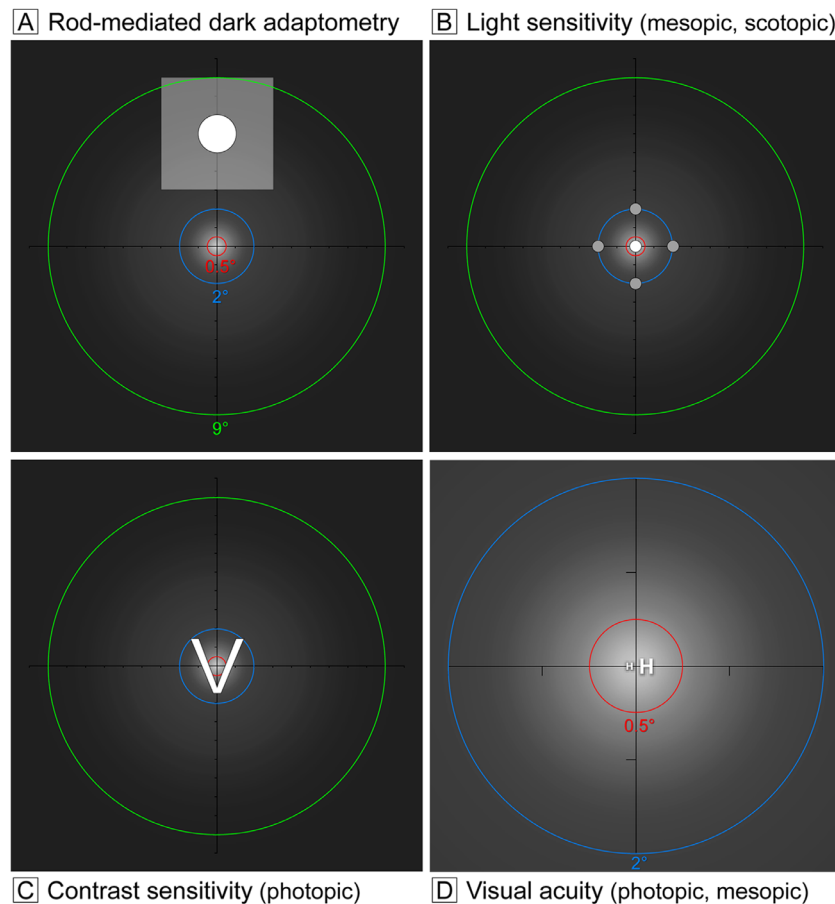


**FIGURE 2.** Relations of visual stimuli to topography of macular xanthophyll pigment. For illustrative purposes, a macular xanthophyll pigment distribution was adapted from that of a male subject imaged by dual-wavelength autofluorescence<sup>59</sup> assuming radial symmetry. Brighter white indicates greater MPOD. Axes cross at fixation, and tick marks indicate 1° intervals. Dashed rings indicate the area over which MPOD was computed by custom software and reported in Table 3. Panels A to C show rings of 1°, 4°, and 18° diameter (0.5°, 2.0°, and 9.0° radius) shown in red, blue, and green, respectively. Panel D shows the two smaller rings only. Rings should not be confused with those that delimit subfields of the ETDRS grid. The terms photopic, scotopic, and mesopic, respectively, refer to vision mediated by cones (in daylight), rods (in starlight), and cones and rods together (at dusk/ dawn). (A) Rod-mediated dark adaptation was assessed 5° superior to the fovea (inferior to the fixation point). The translucent white square represents a 6° square bleaching flash. The solid circle represents a 2° diameter test target. (B) Light sensitivity was measured using microperimetry at points within the central 4° diameter. Mesopic sensitivity was tested at the four gray dots plus the central white dot, for a total of five locations. Scotopic sensitivity was tested at the four gray dots only, due to the absence of rods at fixation. (C) Photopic contrast sensitivity was measured using the Pelli–Robson chart; a sample letter (2.8° square) is shown. (D) Best-corrected visual acuity (small H) and low luminance visual acuity (large H) were measured at fixation and are shown off-center, for clarity. Letters are shown for representative values of these functions in older adults with healthy maculas.<sup>34</sup>

eccentric than other studies<sup>36</sup> and has been recommended,<sup>35</sup> because it avoids high variance due to non-autofluorescent vasculature at greater eccentricities. We measured mean MPOD for the RMDA test spot (radius = 1°, located 5°, or 1.44 mm, directly superior to the fovea). For comparison to horizontally oriented OCT B-scans through the fovea, we determined the mean of all pixels at each eccentricity, within 15° of the horizontal meridian (i.e., within two 30° wedges with the tips at the fovea). The foveal center was taken as the minimum retinal thickness within the central 1-mm diameter (0.5-mm radius) as determined in OCT. As determined using the Spectralis HEYEX software, this is the distance between the inner limiting membrane and the external boundary of the RPE–basal lamina–Bruch’s membrane band.<sup>59</sup>

For comparison of MPOD to regional photoreceptor abundance, published rod and cone densities in flat-mounted normal maculas from human donors 61 to 90 years of age were re-computed from original individual data.<sup>60</sup>

Cone counts have been validated in vivo.<sup>61</sup> Throughout, we used a universal conversion of 0.288 mm per degree of visual angle.<sup>62</sup>

### Statistical Analysis

Data on sample demographics, AMD severity, visual function tests, retinal pathologies, and mean MPOD/MPOV were reported at the eye level. AMD severity was categorized as normal (AREDS 1), early (AREDS 2–4), or intermediate (AREDS 5–8). Visual function measures were compared across AMD severity categories using age-adjusted linear regression. The median and interquartile range were used to summarize the data, as they were not normally distributed. Spearman partial correlations were used to assess the association between visual function measures and MPOD/MPOV accounting for age. MPOD/MPOV values corresponding to the retinal location of each visual function test, as described

**TABLE 1.** Demographic Characteristics and AMD Severity ( $N = 88$ )

Demographic	Value*
Age (y), mean $\pm$ SD	74.9 $\pm$ 5.8
Age group (y), $n$ (%)	
60–69	15 (17.1)
70–79	54 (61.4)
80–89	18 (20.5)
90–100	1 (1.1)
Gender, $n$ (%)	
Male	39 (44.3)
Female	49 (55.7)
Race, $n$ (%)	
White, non-Hispanic	86 (97.7)
African American	1 (1.1)
Asian or Pacific Islander	1 (1.1)
Smoking status, $n$ (%)	
Current	3 (3.4)
Former	41 (46.6)
Never	44 (50.0)
AMD severity, $n$ (%)	
Normal	32 (36.4)
Early	23 (26.1)
Intermediate	33 (37.5)
Lens status, $n$ (%)	
Phakic lens	34 (38.6)
Pseudophakic lens	54 (61.4)

\* Percentages might not sum to 100% due to rounding.

above, were associated with the visual function measure. The level of significance was 0.05. All analyses were completed using SAS 9.4 (SAS Institute, Cary, NC, USA).

## RESULTS

Table 1 shows person-level characteristics of the cohort, which was comprised of 88 individuals (55.7% female and 97.7% white of European descent). Of the 88 eyes tested, 32 (36.4%) were normal, 23 (26.1%) were early AMD, and 33 (37.5%) were intermediate AMD. Phakic eyes represented 36% to 43% and pseudophakic eyes represented 56% to 64% of eyes across the groups of normal and AMD eyes and did not differ among the groups. Current or former smokers represented half of all participants, with similar frequencies among normal subjects and those with early and intermediate AMD (46.9%, 56.5%, and 48.5%, respectively). Table 2 indicates that self-reported oral carotenoid supplement use was higher among subjects with AMD (56.5% and 63.6% in early and intermediate AMD, respectively) than among those with normal maculas ( $P < 0.001$ ). Table 3 presents the results of visual function tests stratified by AMD presence and severity. All visual functions, whether mediated by cones, cones and rods together, or rods only, worsened significantly with increasing AMD severity, after age adjustment.

**TABLE 2.** Self-Reported Oral Carotenoid Supplement Use Stratified by AMD Disease Presence and Severity

	Normal	Early AMD	Intermediate AMD	$P^*$
Supplement use, $n$ (%)				<0.0001
Yes	1 (3.1)	13 (56.5)	21 (63.6)	
No	31 (96.9)	10 (43.5)	12 (36.4)	

\*  $\chi^2$  test.

Table 4 presents regional MPOD, MPOV, rod:cone ratios, and minimum retinal thickness, all stratified by AMD severity. Rod:cone ratios in the fovea, parafovea, and perifovea (as defined in Table 4) were 0, 0.4, and 6.5; in the RMDA test spot at 5° superior on the retina, the ratio was 4.1. As expected, MPOD exhibited a maximum in the fovea and declined with eccentricity for all groups. At the RMDA test spot, MPOD was less than 10% of the maximum in the fovea but did not reach zero (range, 0.011–0.112). MPOD at the RMDA test spot was correlated with MPOD in the parafoveal annulus of the same eyes ( $r = 0.44$ ,  $P < 0.001$ ) but not with MPOD in the fovea ( $r = 0.20$ ,  $P = 0.0644$ ). Median foveal and parafoveal MPOD and MPOV differed by AMD status and severity, with the highest values among those with early and intermediate AMD ( $P < 0.05$  for all). Minimum retinal thickness in the central 1° of the fovea did not vary between AMD presence and severity groups, ranging from 221 to 233  $\mu\text{m}$ .

Table 5 shows age-adjusted associations between visual functions and MPOD in the retinal regions where each test was performed. Although all visual functions worsened in AMD (as shown in Table 3), only some changed in relation to MPOD. Higher MPOD in the central 1°, and not in other regions, was associated with better BCVA ( $r = -0.22$ ,  $P = 0.044$ ) but worse low luminance deficit ( $r = 0.23$ ,  $P = 0.029$ ). Higher MPOD in the area of the RMDA test target, and not in other regions, was associated with faster RMDA ( $r = -0.30$ ,  $P = 0.005$ ). Better contrast sensitivity, measured in the fovea, was associated with higher MPOD at the RMDA test spot at 5° superior ( $r = 0.23$ ,  $P = 0.031$ ). Retinal thickness increased in the central 1° diameter as MPOD increased ( $r = 0.36$ ,  $P < 0.001$ ).

Figure 3 shows representative structural OCT and dual-wavelength autofluorescence imaging of MPOD in a normal eye and eyes with early and intermediate AMD. In all three eyes, the central area with MPOD signal was slightly elongated in the horizontal direction. In OCT images of an older normal eye (Fig. 3A), the outer retinal hyperreflective bands were uniform and regular, and the MPOD distribution had a central peak within an asymmetric ring slightly higher nasally than temporally. An eye with early AMD (Fig. 3B) had an RPE disturbance temporal to the fovea, thinning of foveal ellipsoid zone, and fine stripes of OCT light in the choroid (hypertransmission). This eye exhibited an MPOD peak that was higher and more symmetrical than the normal eye in Figure 3A, with an asymmetric fall-off temporally and patchy signal loss related to the RPE disturbance. An eye with intermediate AMD (Fig. 3C) showed confluent drusen under the fovea and parafovea, subretinal drusenoid deposits (SDDs, magnified in an inset), a high central peak of MPOD, and depressed overall signal superiorly, with patterned spots of deeper loss related to drusen and SDDs. MPOD profiles along the horizontal meridian for all 88 study eyes (computed as described in the Methods section) are shown in Figure 4.

TABLE 3. Age-Adjusted Association of Visual Function with AMD Presence and Severity

	Median (Interquartile Range)			P*
	Normal (n = 32)	Early AMD (n = 23)	Intermediate AMD (n = 33)	
Cone-mediated tests				
Best-corrected visual acuity (logMAR)	-0.01 (-0.06 to 0.09)	-0.02 (-0.08 to 0.04)	0.08 (0.00–0.18)	0.015
Contrast sensitivity (log sensitivity)	1.58 (1.50–1.65)	1.60 (1.60–1.65)	1.50 (1.45–1.60)	<0.001
Cone- and rod-mediated tests				
Low-luminance visual acuity (logMAR)	0.23 (0.14–0.35)	0.26 (0.14–0.48)	0.38 (0.24–0.56)	<0.001
Low-luminance deficit	0.18 (0.16–0.26)	0.24 (0.18–0.40)	0.28 (0.22–0.34)	0.004
Mesopic light sensitivity (dB)†	23.60 (20.40–28.80)	24.20 (21.80–26.40)	20.40 (17.50–22.80)	<0.001
Rod-mediated tests				
Scotopic light sensitivity (dB)†	12.00 (10.40–14.40)	13.00 (10.80–13.80)	9.90 (6.70–11.90)	<0.001
Rod intercept time (min)	11.96 (10.28–14.39)	12.02 (9.33–17.90)	20.63 (14.22–28.46)	<0.001

\* Age-adjusted linear regression.

† Some participants did not complete these tests (n = 74).

TABLE 4. Age-Adjusted Association of Macular Xanthophyll Pigment and Foveal Thickness with AMD Presence and Severity

	Median (Interquartile Range)			P*
	Normal (n = 32)	Early AMD (n = 23)	Intermediate AMD (n = 33)	
Mean MPOD (region, rod:cone ratio)†				
0–0.5° (fovea, 0)	0.51 (0.37–0.64)	0.67 (0.52–0.79)	0.65 (0.55–0.79)	0.024
0.5–2.0° (parafovea, 0.4)	0.27 (0.22–0.35)	0.30 (0.22–0.46)	0.35 (0.32–0.43)	0.015
2.0–9.0° (perifovea, 6.5)	0.05 (0.03–0.05)	0.06 (0.03–0.08)	0.05 (0.04–0.06)	0.053
RMDA test spot (5° superior perifovea, 4.1)	0.04 (0.03–0.05)	0.05 (0.04–0.07)	0.04 (0.03–0.05)	0.158
Mean MPOV‡ (region, rod:cone ratio)				
0.0–2.0° (central macula, 0.4)	0.30 (0.23–0.41)	0.34 (0.26–0.53)	0.40 (0.36–0.48)	0.012
0.0–9.0° (macula, 5.5)	1.30 (0.95–1.51)	1.59 (1.00–2.17)	1.50 (1.12–1.64)	0.025
Minimum retinal thickness (0°–0.5°)	220.5 (209.0–236.0)	233.0 (209.0–250.0)	221.0 (208.0–242.0)	0.260

\* Age-adjusted linear regression.

† Retinal regions are described in terms of radius (eccentricity from the foveal center). Rod:cone ratios were recently re-computed from digital maps of histologic photoreceptor topography for donors 61 to 90 years of age for regions of the ETDRS grid, as described elsewhere,<sup>60</sup> and for regions of interest for the MPOD distribution as described herein.‡ MPOV = MPOD × mm<sup>2</sup>.

TABLE 5. Associations† of Macular Xanthophyll Pigment with Visual Function and Minimum Retinal Thickness (N = 88)

	MPOD 1°-Diameter Disk Centered on Fovea		MPOD at RMDA Test Spot		MPOV 4°-Diameter Disk Centered on Fovea	
	Correlation Coefficient	P	Correlation Coefficient	P	Correlation Coefficient	P
Cone-mediated tests						
Best-corrected visual acuity (logMAR)	<b>-0.22</b>	<b>0.044*</b>	-0.14	0.202	-0.10	0.350
Contrast sensitivity (log sensitivity)	0.12	0.287	<b>0.23</b>	<b>0.031*</b>	0.04	0.700
Cone- and rod-mediated tests						
Low-luminance visual acuity (logMAR)	-0.01	0.898	-0.15	0.179	0.03	0.804
Low-luminance deficit	<b>0.23</b>	<b>0.029*</b>	-0.05	0.065	0.19	0.075
Mesopic light sensitivity (dB)‡	0.08	0.513	0.17	0.156	-0.07	0.562
Rod-mediated tests						
Scotopic light sensitivity (dB)‡	0.08	0.509	0.12	0.301	-0.19	0.115
Rod intercept time (min)	0.19	0.079	<b>-0.30</b>	<b>0.005*</b>	0.20	0.065
Minimum retinal thickness (µm)§	<b>0.36</b>	<b>&lt;0.001*</b>	-0.14	0.184	-0.06	0.604

\* Indicates statistical significance at P &lt; 0.05 (bold).

† Spearman partial correlation coefficient, adjusted for age.

‡ Some participants did not complete these tests (n = 74).

§ Measured using the automated internal limiting membrane (ILM)-RPE segmentation of the Heidelberg HEYEX software.

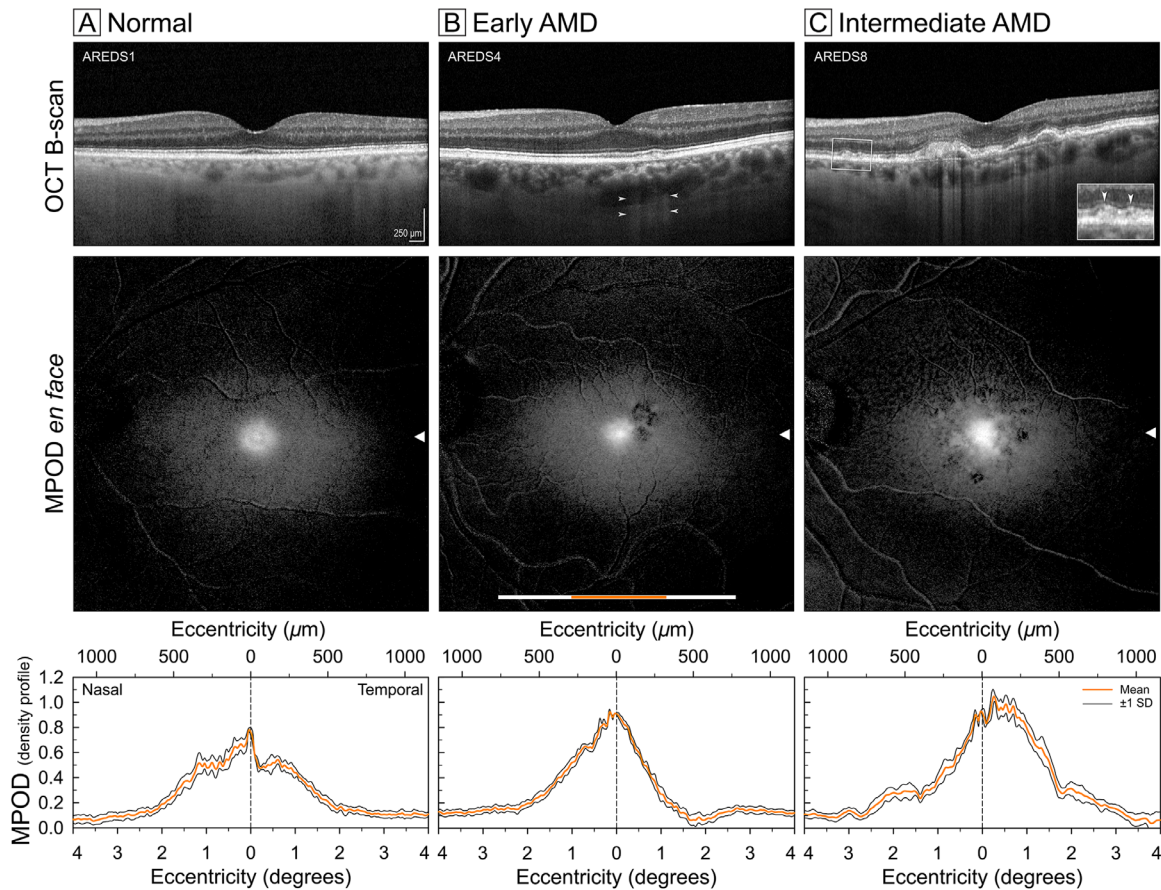


**FIGURE 3.** Structural and macular xanthophyll pigment imaging in eyes with and without early and intermediate AMD. Comparison of foveal OCT B-scans (top row), spatial distribution of xanthophyll carotenoids using dual-wavelength autofluorescence (middle row), and profile distribution of MPOD (bottom row) in a representative aged normal (A), early AMD (B), and intermediate AMD eye, with AREDS stages indicated. The white scale bar in the en face image represents the x-location and extent of the 20° OCT B-scan. The orange scale bar overlay represents the extent of 8° MPOD density sampled from two 30°-wide wedges centered on the fovea (resembling a bowtie). A conversion factor of 0.288 mm/° of visual angle is used. Arrowheads represent corresponding fovea-centered y-locations for the scans and plots. Scale bar: 250 μm (top panels). OCT in top row shows AMD pathology in B (RPE disturbance, arrowheads indicating pinstripe hypertransmission) and C (drusen, pinstripe hypertransmission, and, in a magnified inset, subretinal drusenoid deposit).

## DISCUSSION

In normal and AMD eyes in persons in the southeastern United States, we found that higher foveal MPOD assessed with dual-wavelength autofluorescence is associated with better photopic acuity and greater thickness of central fovea. For the first time, to the best of our knowledge, we also directly determined MPOD at a superior perifoveal RMDA test location. Overall values were low and unrelated to AMD severity, yet positively associated with faster RMDA. MPOD measures were not associated with most other visual functions, due to either sample size or the nature of the neurophysiology underlying these tests, or both. Associations of foveal MPOD with low-luminance deficit (involving rods) and perifoveal MPOD with foveal contrast sensitivity are counterintuitive and should be evaluated in a larger sample. Our findings have implications for vision, xanthophyll biology, AMD pathogenesis, and dual-wavelength autofluorescence imaging.

A positive association of foveal MPOD with BCVA builds on prior research in which tissue-level MPOD was assessed with HFP<sup>6,24,30,31,63,64</sup> and other techniques.<sup>65,66</sup> In younger adults with normal maculas, BCVA is modestly associated

with higher MPOD<sup>24</sup> and has been shown to improve 6 to 12 months after supplementation in some studies<sup>6,31,63</sup> but not in others.<sup>30,64</sup> In eyes with variably defined AMD, BCVA improved with supplementation in relation to MPOD in some studies<sup>65–67</sup> but not in others.<sup>31,68–70</sup> Although our study eyes were staged by CFP, for statistical purposes we pooled aged normal and AMD eyes (Table 5) due to sample size, as previous investigators have done.<sup>67,69,70</sup> Significant associations have been described as explaining little of the variance,<sup>24,67</sup> as was also true for our data ( $r^2 = 0.05$ ). The idea that yellow MP could improve acuity is long standing, dating back to Schultz in 1866,<sup>71,72</sup> and has appeal because cone spacing limits foveal acuity,<sup>73,74</sup> and these cones are interleaved with Müller glia.<sup>75</sup> However, the original idea that xanthophylls improve acuity by filtering blue light and reducing chromatic aberration has taken a back seat to other ideas, as discussed below.

One striking and apparently novel finding is higher levels of MPOD, in early and intermediate AMD compared to normal eyes, by all measures as assessed by objective imaging. Previous studies, all small like ours, have reported that MPOD was the same (Ireland),<sup>69,76,77</sup> or lower (South Korea)<sup>78</sup> in AMD eyes when compared to normal eyes. These

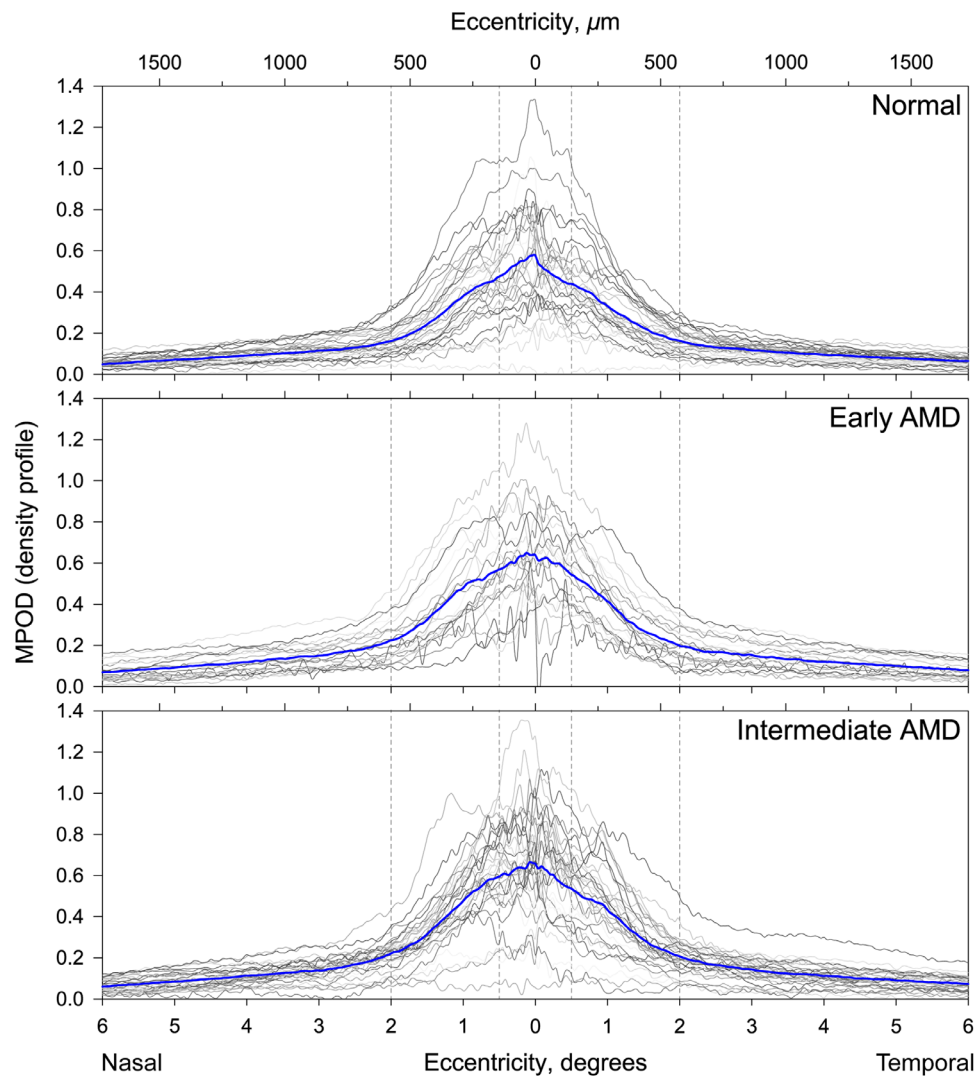


**FIGURE 4.** Density profiles showing macular xanthophyll pigment distribution in individual eyes with and without early and intermediate AMD. The *gray lines* represent individual 12° MPOD density profiles sampled from two wedges (resembling a bowtie) centered on the fovea in 32 normal, 23 early AMD, and 33 intermediate AMD eyes. The *blue lines* represent the mean MPOD density profiles for the respective groups. A conversion factor of 0.288 mm/° of visual angle is used.

findings were obtained by HFP at single<sup>77,78</sup> or several<sup>69,76</sup> retinal test locations. Short-term supplementation trials in AMD eyes have found that BCVA improves months after an MPOD increase,<sup>6,63,65</sup> leading to the conclusion that this lag could not be solely attributable to an increase in optical filtration.<sup>66</sup> Interestingly, supplementation use and MPOD abundance in our study were higher in early AMD eyes than in normal eyes, and upticks in cone-mediated vision were largest at intermediate AMD (Table 3). It is possible that dual-wavelength autofluorescence imaging used in our study revealed a long-term, tissue-level benefit of supplementation (e.g., involving modified gene expression). This idea remains speculative without more information about supplement onset and serum xanthophyll concentrations in our sample. Supplement use may also be a surrogate for factors we did not assess (e.g., overall better attention to health).

We found that increased MPOD abundance was associated with faster RMDA despite being <10% of peak values at the foveal center. It could be argued that a sufficiently high

level of MP at 5° eccentricity could delay RMDA simply by reducing the intensity of light reaching the photoreceptors,<sup>77</sup> but we found the reverse. Low values of MPOD at the RMDA test location in our study suggest that light filtration is not a major factor. Other investigators reported both positive<sup>5</sup> and negative<sup>27,31</sup> associations of MPOD regarding aspects of rod-mediated visual tasks distinct from retinoid-limited RMDA used in this study. As mentioned above, an association of delayed RMDA with low MPOD measured with HFP at fixation was found with a small sample and under non-standard stimulus conditions.<sup>33</sup> We did not confirm this association in a much larger sample ( $N = 306$ ) under standard conditions.<sup>34</sup> In the current study, we assessed local MPOD at the RMDA test spot using objective and unbiased dual-wavelength autofluorescence imaging. Indeed, small and functionally significant changes in MPOD at this location would not be detectable in a global measure that also included high foveal values. This association with RMDA was modest and could be real or represent a surrogate for other aspects of MP biology in these eyes, as explored below.

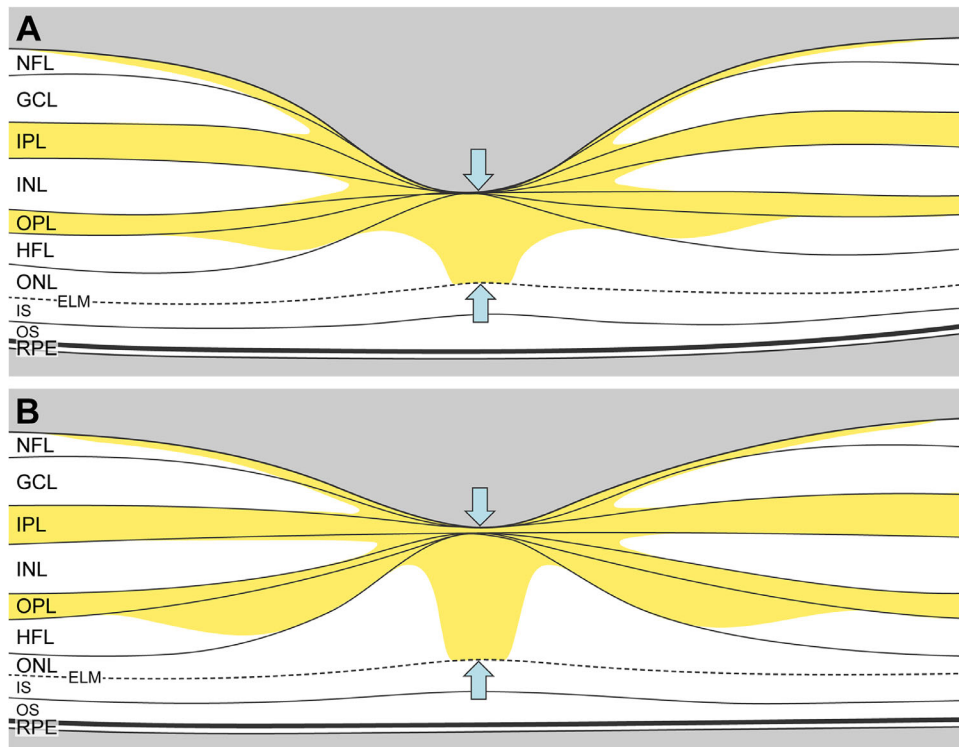


**FIGURE 5.** Schematic representation of macular xanthophyll pigment distribution in thick versus thin foveas. The macular xanthophyll pigment distribution from Snodderly et al.<sup>18</sup> shows abundant pigment in the inner and outer plexiform layers and the Henle fiber layer. (A) This schematic illustration shows how the central macular xanthophyll pigment could appear lower in thin fovea with a small, deep pit due to the smaller central bouquet (blue arrows). (B) In contrast, a thicker fovea with a wider, shallow pit would have more macular xanthophyll pigment due to a more extensive central bouquet (blue arrows) comprised of cones and Müller cells. Thick and thin foveas were defined by described methods.<sup>100</sup>

Can one mechanism explain the association of higher MPOD with better BCVA and RMDA? We offer a scenario in which the vertical and lateral components of the MP distribution (Fig. 5) play separate roles via variations in foveal shape, previously suggested as risk factors.<sup>79</sup> A recently articulated center-surround model of cone resilience and rod vulnerability in aging and AMD incorporates a barrier to retinoid transport in the choriocapillaris–Bruch’s membrane–RPE complex.<sup>10,80,81</sup> In brief, the RPE constitutively secretes lipoproteins to the circulation to offload unneeded lipids. During aging, the exit route across Bruch’s membrane and choriocapillaris endothelium gradually fails, resulting in lipid-rich drusen in many older eyes. Perifoveal rods are harmed as lipids accumulate in Bruch’s membrane, blocking exchange. Foveal cones themselves are relatively spared, because the Müller glia protecting them are also supplied from retinal vasculature.

Regarding the vertical component, a high MPOD concentration in the central-most cones and Müller cells potentially enhances cone-mediated BCVA while also concentrating vertically orienting lipid trafficking into the foveal center, increasing the amount of lipid disposed by RPE directly below. Accordingly, and in agreement with some studies<sup>82–85</sup> but not others,<sup>86,87</sup> we found higher MPOD associated with foveas that were 5.4% thicker (schematized in Fig. 5). Over a lifespan, this significant but small anatomic difference may have a biologic impact,<sup>79</sup> just as gene sequence variants are believed to affect the efficiency of molecular interactions. Recently Obana et al.<sup>11</sup> found a strong positive relationship between MPOD and the distance

between foveal inner and external limiting membranes in older Japanese adults with normal maculas and low supplement usage. The foveal center contains numerous Müller glia,<sup>75</sup> including distinct populations likely accounting for a long-sought Müller cell “cone” of high xanthophyll content.<sup>88</sup>

The impact of xanthophyll spatial distribution on RMDA may involve foveal shape and the lateral extent of glial processes in the plexiform layers (Fig. 5). We previously hypothesized that plasma high-density lipoproteins (HDL) bearing MP taken up by the RPE for transfer to neurosensory retina is a candidate source for fatty acids in Bruch’s membrane lipids.<sup>10</sup> In this model, lipid trafficking to glial processes may relate to the lateral extent of drusen material and barrier dysfunction under central macula.<sup>89,90</sup> A thick fovea (Fig. 5B) with more lipid directly beneath it may have less lipid at the RMDA test spot and vice versa for a thin fovea (Fig. 5A). Thus, higher foveal MPOD may reduce harm to parafoveal rods by centrally concentrating excess lipid in and around the fovea (Fig. 5) while enhancing cone-mediated foveal vision. This idea would be supported by an association between foveal and perifoveal MPOD, which we did not detect (Table 5). However, an eccentricity-dependent gradient of Müller glia phenotypes distinguishable by morphology and xanthophyll content is suggested by independent effects on foveal and perifoveal MPOD in macular telangiectasia type 2.<sup>91</sup> More data from larger samples are needed; linking retinal layers to en face dual-wavelength autofluorescence images of MPOD in individual eyes will be informative.

With the detailed dual-wavelength autofluorescence images for AMD that we obtained (Fig. 3), we can opine as to this modality's utility. Dual-wavelength autofluorescence imaging has two major assumptions<sup>92</sup> that should be updated in light of new information about the subcellular and cellular basis of RPE autofluorescence. One assumption is that the excitation spectra of RPE signal sources (e.g., lipofuscin) are the same at different retinal locations. Although this assumption seems reasonable at the organelle level, it is now known that human RPE organelle content varies with region. Melanolipofuscin is more abundant than lipofuscin under the fovea,<sup>40</sup> and its spectrum may differ from that of lipofuscin.<sup>93</sup> Further, how loss and rearrangement of RPE autofluorescent granules in AMD<sup>38,39</sup> affect the balance of excitation spectra remains to be determined. Another assumption<sup>92</sup> is that autofluorescence signal is attenuated by only MP, implying an absence of additional fluorophores, reflectors, or absorbers in retinal layers between the signal sources and detector. It is now known that RPE autofluorescence intensity is modulated by non-RPE tissue layers; for example, shortening of photoreceptors reduces the absorption of incoming excitation light, resulting in hyperautofluorescence.<sup>94</sup> A major unknown is how reactive gliosis in AMD<sup>95,96</sup> might impact the xanthophyll content of Müller cell membranes. Thus, MPOD imaging in AMD will be most useful when co-registered with OCT imaging for a multilayer understanding of signal sources and modulators.

Strengths of this study are its objective and unbiased imaging method for MPOD, tests of rod and cone function with different neurophysiologic bases, new metrics for MPOD that probe visually stimulated regions, defined AMD and control groups, development of a new understanding of RPE autofluorescence, and a theory that links soft drusen to MP and macular Müller glia.<sup>10</sup> Limitations include a small sample size that reduced statistical power, lack of details on lens density in phakic eyes and posterior subcapsular opacification in pseudophakic eyes, and lack of supplement history to inform conclusions about autofluorescence signal strength and tissue xanthophyll content. Additional limitations include use of a CFP-based grading scale for AMD severity that does not cover the full range of known AMD pathology, lack of information about individual differences in axial length and foveal shape that impact measurement accuracy in en face images,<sup>97</sup> and lack of genetic testing especially for HDL genes implicated in AMD risk.<sup>98</sup>

In conclusion, our study has documented macular xanthophyll abundance and rod- and cone-mediated vision in perhaps the most comprehensive manner to date while incorporating new theories of AMD deposit pathogenesis and human visual neuroscience. Our data have clinical relevance in showing that higher MPOD at foveal and parafoveal locations in older people is associated with better cone-mediated acuity and RMDA, respectively. Further investigation of dual-wavelength autofluorescence imaging is warranted, especially in conditions where Müller glia involvement is suspected. Many questions raised in this study will be addressed in a large prospective observational trial (ALSTAR2, NCT04112667) that is ongoing.<sup>81</sup>

### Acknowledgments

The authors thank Joseph Carroll, PhD (Medical College of Wisconsin) for exemplar OCT scans of thick and thin foveas used for the schematic illustrations in Figure 5.

Supported by National Institutes of Health Grants (R01AG04212, R01EY029595, and R01EY027948); EyeSight Foundation of Alabama; Dorsett Davis Discovery Fund; Alfreda J. Schueler Trust; Research to Prevent Blindness, Inc.; and Heidelberg Engineering.

Disclosure: **D. Kar**, None; **M.E. Clark**, None; **T.A. Swain**, None; **G. McGwin Jr.**, None; **J.N. Crosson**, None; **C. Owsley**, (P); **K.R. Sloan**, MacRegen (I); **C.A. Curcio**, Heidelberg Engineering (F), Genentech/Hoffman LaRoche (F), MacRegen (I)

### References

1. Flaxman SR, Bourne RRA, Resnikoff S, et al. Global causes of blindness and distance vision impairment 1990-2020: a systematic review and meta-analysis. *Lancet Glob Health*. 2017;5:e1221–e1234.
2. Bernstein PS, Li B, Vachali PP, et al. Lutein, zeaxanthin, and meso-zeaxanthin: the basic and clinical science underlying carotenoid-based nutritional interventions against ocular disease. *Prog Retin Eye Res*. 2016;50:34–66.
3. Age-Related Eye Disease Study 2 Research Group. Lutein + zeaxanthin and omega-3 fatty acids for age-related macular degeneration: the Age-Related Eye Disease Study 2 (AREDS2) randomized clinical trial. *JAMA*. 2013;309:2005–2015.
4. Loane E, Nolan JM, O'Donovan O, Bhosale P, Bernstein PS, Beatty S. Transport and retinal capture of lutein and zeaxanthin with reference to age-related macular degeneration. *Surv Ophthalmol*. 2008;53:68–81.
5. Stringham JM, Garcia PV, Smith PA, et al. Macular pigment and visual performance in low-light conditions. *Invest Ophthalmol Vis Sci*. 2015;56:2459–2468.
6. Nolan JM, Loughman J, Akkali MC, et al. The impact of macular pigment augmentation on visual performance in normal subjects: COMPASS. *Vision Res*. 2011;51:459–469.
7. Renzi LM, Hammond BR, Jr. The relation between the macular carotenoids, lutein and zeaxanthin, and temporal vision. *Ophthalmic Physiol Opt*. 2010;30:351–357.
8. Erdman JW, Jr, Smith JW, Kuchan MJ, et al. Lutein and brain function. *Foods*. 2015;4:547–564.
9. Mohn ES, Erdman JW, Jr, Kuchan MJ, Neuringer M, Johnson EJ. Lutein accumulates in subcellular membranes of brain regions in adult rhesus macaques: relationship to DHA oxidation products. *PLoS One*. 2017;12:e0186767.
10. Curcio CA. Antecedents of soft drusen, the specific deposit of age-related macular degeneration, in the biology of human macula. *Invest Ophthalmol Vis Sci*. 2018;59:AMD182–AMD194.
11. Obana A, Gohto Y, Sasano H, et al. Spatial distribution of macular pigment estimated by autofluorescence imaging in elderly Japanese individuals. *Jpn J Ophthalmol*. 2020;64:160–170.
12. Helb H-M, Issa PC, van der Veen RLP, Berendschot TTJM, Scholl HPN, Holz FG. Abnormal macular pigment distribution in type 2 idiopathic macular telangiectasia. *Retina*. 2008;28:808–816.
13. Powner MB, Gillies MC, Tretiach M, et al. Perifoveal Müller cell depletion in a case of macular telangiectasia type 2. *Ophthalmology*. 2010;117:2407–2416.
14. Powner MB, Gillies MC, Zhu M, Vevis K, Hunyor AP, Frutiger M. Loss of Müller's cells and photoreceptors in macular telangiectasia type 2. *Ophthalmology*. 2013;120:2344–2352.
15. Theelen T, Berendschot TT, Klevering BJ, Fuijkschot J, Hoyng CB, Willemsen MA. Multimodal imaging of the macula in hereditary and acquired lack of macular pigment. *Acta Ophthalmol*. 2014;92:138–142.

16. Pang CE, Maberley DA, Freund KB, et al. Lamellar hole-associated epiretinal proliferation: a clinicopathologic correlation. *Retina*. 2016;36:1408–1412.
17. Obana A, Sasano H, Okazaki S, Otsuki Y, Seto T, Gohto Y. Evidence of carotenoid in surgically removed lamellar hole-associated epiretinal proliferation. *Invest Ophthalmol Vis Sci*. 2017;58:5157–5163.
18. Snodderly DM, Auran JD, Delori FC. The macular pigment. II. Spatial distribution in primate retinas. *Invest Ophthalmol Vis Sci*. 1984;25:674–685.
19. Trieschmann M, van Kuijk FJ, Alexander R, et al. Macular pigment in the human retina: histological evaluation of localization and distribution. *Eye (Lond)*. 2008;22:132–137.
20. Li B, George EW, Rognon GT, et al. Imaging lutein and zeaxanthin in the human retina with confocal resonance Raman microscopy. *Proc Natl Acad Sci USA*. 2020;117:12352–12358.
21. Liu A, Chang J, Lin Y, Shen Z, Bernstein PS. Long-chain and very long-chain polyunsaturated fatty acids in ocular aging and age-related macular degeneration. *J Lipid Res*. 2011;51:3217–3229.
22. Perry VH, Cowey A. The lengths of the fibres of Henle in the retina of macaque monkeys: implications for vision. *Neuroscience*. 1988;25:225–236.
23. Li M, Huisingh C, Messinger JD, et al. Histology of geographic atrophy secondary to age-related macular degeneration: a multilayer approach. *Retina*. 2018;38:1937–1953.
24. Loughman J, Akkali MC, Beatty S, et al. The relationship between macular pigment and visual performance. *Vision Res*. 2010;50:1249–1256.
25. Stringham JM, Hammond BR. Macular pigment and visual performance under glare conditions. *Optom Vis Sci*. 2008;85:82–88.
26. Bovier ER, Renzi LM, Hammond BR. A double-blind, placebo-controlled study on the effects of lutein and zeaxanthin on neural processing speed and efficiency. *PLoS One*. 2014;9:e108178.
27. Hammond BR, Jr, Wooten BR, Snodderly DM. Preservation of visual sensitivity of older subjects: association with macular pigment density. *Invest Ophthalmol Vis Sci*. 1998;39:397–406.
28. Hammond BR, Fletcher LM, Roos F, Wittwer J, Schalch W. A double-blind, placebo-controlled study on the effects of lutein and zeaxanthin on photostress recovery, glare disability, and chromatic contrast. *Invest Ophthalmol Vis Sci*. 2014;55:8583–8589.
29. Kvensakul J, Rodriguez-Carmona M, Edgar DF, et al. Supplementation with the carotenoids lutein or zeaxanthin improves human visual performance. *Ophthalmic Physiol Opt*. 2006;26:362–371.
30. Yao Y, Qiu QH, Wu XW, Cai ZY, Xu S, Liang XQ. Lutein supplementation improves visual performance in Chinese drivers: 1-year randomized, double-blind, placebo-controlled study. *Nutrition*. 2013;29:958–964.
31. van der Made SM, Kelly ER, Kijlstra A, Plat J, Berendschot TT. Increased macular pigment optical density and visual acuity following consumption of a buttermilk drink containing lutein-enriched egg yolks: a randomized, double-blind, placebo-controlled trial. *J Ophthalmol*. 2016;2016:9035745.
32. Rodriguez-Carmona M, Kvensakul J, Harlow JA, Kopcke W, Schalch W, Barbur JL. The effects of supplementation with lutein and/or zeaxanthin on human macular pigment density and colour vision. *Ophthalmic Physiol Opt*. 2006;26:137–147.
33. Patryas L, Parry NR, Carden D, Aslam T, Murray IJ. The association between dark adaptation and macular pigment optical density in healthy subjects. *Graefes Arch Clin Exp Ophthalmol*. 2014;252:657–663.
34. Zarubina AV, Huisingh CE, Clark ME, et al. Rod-mediated dark adaptation and macular pigment optical density in older adults with normal maculas. *Curr Eye Res*. 2018;43:913–920.
35. Conrady CD, Bell JP, Besch BM, et al. Correlations between macular, skin, and serum carotenoids. *Invest Ophthalmol Vis Sci*. 2017;58:3616–3627.
36. Green-Gomez M, Bernstein PS, Curcio CA, Moran R, Roche W, Nolan JM. Standardizing the assessment of macular pigment using a dual-wavelength autofluorescence technique. *Transl Vis Sci Technol*. 2019;8:41.
37. Ach T, Huisingh C, McGwin G, Jr, et al. Quantitative autofluorescence and cell density maps of the human retinal pigment epithelium. *Invest Ophthalmol Vis Sci*. 2014;55:4832–4841.
38. Ach T, Tolstik E, Messinger JD, Zarubina AV, Heintzmann R, Curcio CA. Lipofuscin re-distribution and loss accompanied by cytoskeletal stress in retinal pigment epithelium of eyes with age-related macular degeneration. *Invest Ophthalmol Vis Sci*. 2015;56:3242–3252.
39. Gamberil JA, Sloan KR, Swain TA, et al. Quantifying retinal pigment epithelium dysmorphia and loss of histologic autofluorescence in age-related macular degeneration. *Invest Ophthalmol Vis Sci*. 2019;60:2481–2493.
40. Bermond K, Wobbe C, Tarau IS, et al. Autofluorescent granules of the human retinal pigment epithelium: age-related topographic and intracellular distribution. *Invest Ophthalmol Vis Sci*. 2020;61:35.
41. Crosson JN, Swain TA, Clark ME, et al. Retinal pathologic features on OCT among eyes of older adults judged healthy by color fundus photography. *Ophthalmol Retina*. 2019;3:670–680.
42. Age-Related Eye Disease Study Research Group. The Age-Related Eye Disease Study severity scale for age-related macular degeneration: AREDS Report No. 17. *Arch Ophthalmol*. 2005;123:1484–1498.
43. Vitale S, Clemons TE, Agron E, et al. Evaluating the validity of the Age-Related Eye Disease Study Grading Scale for age-related macular degeneration: AREDS2 Report 10. *JAMA Ophthalmol*. 2016;134:1041–1047.
44. Querques G, Srour M, Massamba N, et al. Functional characterization and multimodal imaging of treatment-naive “quiescent” choroidal neovascularization. *Invest Ophthalmol Vis Sci*. 2013;54:6886–6892.
45. Roisman L, Zhang Q, Wang RK, et al. Optical coherence tomography angiography of asymptomatic neovascularization in intermediate age-related macular degeneration. *Ophthalmology*. 2016;123:1309–1319.
46. Shi Y, Motulsky EH, Goldhardt R, et al. Predictive value of the OCT double-layer sign for identifying subclinical neovascularization in age-related macular degeneration. *Ophthalmol Retina*. 2019;3:211–219.
47. Owsley C, Huisingh C, Jackson GR, et al. Associations between abnormal rod-mediated dark adaptation and health and functioning in older adults in normal macular health. *Invest Ophthalmol Vis Sci*. 2014;55:4776–4789.
48. Owsley C, McGwin G, Jr, Clark ME, et al. Delayed rod-mediated dark adaptation is a functional biomarker for incident early age-related macular degeneration. *Ophthalmology*. 2016;123:344–351.
49. Jackson GR, Edwards JG. A short-duration dark adaptation protocol for assessment of age-related maculopathy. *J Ocul Biol Dis Infor*. 2008;1:7–11.
50. Lamb TD, Pugh EN, Jr. Dark adaptation and the retinoid cycle of vision. *Prog Retin Eye Res*. 2004;23:307–380.

51. Owsley C, Huisinigh C, Clark ME, Jackson GR, McGwin G, Jr. Comparison of visual function in older eyes in the earliest stages of age-related macular degeneration to those in normal macular health. *Curr Eye Res.* 2016;41:266–272.
52. Beck RW, Moke PS, Turpin AH, et al. A computerized method of visual acuity testing: adaptation of the early treatment of diabetic retinopathy study testing protocol. *Am J Ophthalmol.* 2003;135:194–205.
53. Sunness JS, Rubin GS, Applegate CA, et al. Visual function abnormalities and prognosis in eyes with age-related geographic atrophy of the macula and good visual acuity. *Ophthalmology.* 1997;104:1677–1691.
54. Pelli DG, Robson JG, Wilkins AJ. The design of a new letter chart for measuring contrast sensitivity. *Clin Vision Sci.* 1988;2:197–199.
55. Elliott DB, Bullimore MA, Bailey IL. Improving the reliability of the Pelli-Robson contrast sensitivity test. *Clin Vision Sci.* 1991;6:471–475.
56. Steinberg JS, Sassmannshausen M, Fleckenstein M, et al. Correlation of partial outer retinal thickness with scotopic and mesopic fundus-controlled perimetry in patients with reticular drusen. *Am J Ophthalmol.* 2016;168:52–61.
57. Steinberg JS, Fitzke FW, Fimmers R, Fleckenstein M, Holz FG, Schmitz-Valckenberg S. Scotopic and photopic microperimetry in patients with reticular drusen and age-related macular degeneration. *JAMA Ophthalmol.* 2015;133:690–697.
58. Schindelin J, Arganda-Carreras I, Frise E, et al. Fiji: an open-source platform for biological-image analysis. *Nat Methods.* 2012;9:676–682.
59. Giani A, Cigada M, Choudhry N, et al. Reproducibility of retinal thickness measurements on normal and pathologic eyes by different optical coherence tomography instruments. *Am J Ophthalmol.* 2010;150:815–824.
60. Curcio CA, Millican CL, Allen KA, Kalina RE. Aging of the human photoreceptor mosaic: evidence for selective vulnerability of rods in central retina. *Invest Ophthalmol Vis Sci.* 1993;34:3278–3296.
61. Zhang T, Godara P, Blanco ER, et al. Variability in human cone topography assessed by adaptive optics scanning laser ophthalmoscopy. *Am J Ophthalmol.* 2015;160:290–300.e291.
62. Drasdo N, Fowler CW. Non-linear projection of the retinal image in a wide-angle schematic eye. *Br J Ophthalmol.* 1974;58:709–714.
63. Loughman J, Nolan JM, Howard AN, Connolly E, Meagher K, Beatty S. The impact of macular pigment augmentation on visual performance using different carotenoid formulations. *Invest Ophthalmol Vis Sci.* 2012;53:7871–7880.
64. Nolan JM, Power R, Stringham J, et al. Enrichment of macular pigment enhances contrast sensitivity in subjects free of retinal disease: Central Retinal Enrichment Supplementation Trials - Report 1. *Invest Ophthalmol Vis Sci.* 2016;57:3429–3439.
65. Dawczynski J, Jentsch S, Schweitzer D, Hammer M, Lang GE, Strobel J. Long term effects of lutein, zeaxanthin and omega-3-LCPUFAs supplementation on optical density of macular pigment in AMD patients: the LUTEGA study. *Graefes Arch Clin Exp Ophthalmol.* 2013;251:2711–2723.
66. Weigert G, Kaya S, Pemp B, et al. Effects of lutein supplementation on macular pigment optical density and visual acuity in patients with age-related macular degeneration. *Invest Ophthalmol Vis Sci.* 2011;52:8174–8178.
67. Puell MC, Palomo-Alvarez C, Barrio AR, Gomez-Sanz FJ, Perez-Carrasco MJ. Relationship between macular pigment and visual acuity in eyes with early age-related macular degeneration. *Acta Ophthalmol.* 2013;91:e298–303.
68. Akuffo KO, Nolan JM, Howard AN, et al. Sustained supplementation and monitored response with differing carotenoid formulations in early age-related macular degeneration. *Eye (Lond).* 2015;29:902–912.
69. Akuffo KO, Beatty S, Peto T, et al. The impact of supplemental antioxidants on visual function in nonadvanced age-related macular degeneration: a head-to-head randomized clinical trial. *Invest Ophthalmol Vis Sci.* 2017;58:5347–5360.
70. Akuffo KO, Nolan JM, Peto T, et al. Relationship between macular pigment and visual function in subjects with early age-related macular degeneration. *Br J Ophthalmol.* 2017;101:190–197.
71. Schultze M. Zur Anatomie und Physiologie der Retina. *Arch f mikroskop Anat.* 1866;2:165–286.
72. Engles M, Wooten B, Hammond B. Macular pigment: a test of the acuity hypothesis. *Invest Ophthalmol Vis Sci.* 2007;48:2922–2931.
73. Hirsch J, Curcio CA. The spatial resolution capacity of the human fovea. *Vision Res.* 1989;29:1095–1101.
74. Rossi EA, Roorda A. The relationship between visual resolution and cone spacing in the human fovea. *Nat Neurosci.* 2010;13:156–157.
75. Ahmad KM, Klug K, Herr S, Sterling P, Schein S. Cell density ratios in a foveal patch in macaque retina. *Vis Neurosci.* 2003;20:189–209.
76. Thurnham DI, Nolan JM, Howard AN, Beatty S. Macular response to supplementation with differing xanthophyll formulations in subjects with and without age-related macular degeneration. *Graefes Arch Clin Exp Ophthalmol.* 2015;253:1231–1243.
77. Beirne RO, McConnell E. Investigation of the relationship between macular pigment levels and rod-mediated dark adaptation in intermediate age-related macular degeneration. *Clin Exp Optom.* 2019;102:611–616.
78. Hong IH, Jung WH, Lee JH, Chang IB. Macular pigment optical density in the Korean population: a cross sectional study. *J Korean Med Sci.* 2020;35:e30.
79. Wagner-Schuman M, Dubis AM, Nordgren RN, et al. Race- and sex-related differences in retinal thickness and foveal pit morphology. *Invest Ophthalmol Vis Sci.* 2011;52:625–634.
80. Curcio CA. Soft drusen in age-related macular degeneration: biology and targeting, via the Oil Spill Strategy. *Invest Ophthalmol Vis Sci.* 2018;59:AMD160–AMD181.
81. Curcio CA, McGwin G, Sadda SR, et al. Functionally validated imaging endpoints in the Alabama Study on Early Age-Related Macular Degeneration 2 (ALSTAR2): design and methods. *BMC Ophthalmol.* 2020;20:196.
82. Liew SH, Gilbert CE, Spector TD, et al. Central retinal thickness is positively correlated with macular pigment optical density. *Exp Eye Res.* 2006;82:915–920.
83. van der Veen RLP, Ostendorf S, Hendrikse F, Berendschot TTJM. Macular pigment optical density relates to foveal thickness. *Eur J Ophthalmol.* 2009;19:836–841.
84. Meyer zu Westrup V, Dietzel M, Pauleikhoff D, Hense H-W. The association of retinal structure and macular pigment distribution. *Invest Ophthalmol Vis Sci.* 2014;55:1169–1175.
85. Ctori I, Huntjens B. The association between foveal morphology and macular pigment spatial distribution: an ethnicity study. *PLoS One.* 2017;12:e0169520.
86. Nolan JM, Stringham JM, Beatty S, Snodderly DM. Spatial profile of macular pigment and its relationship to foveal architecture. *Invest Ophthalmol Vis Sci.* 2008;49:2134–2142.
87. Kirby ML, Galea M, Loane E, Stack J, Beatty S, Nolan JM. Foveal anatomic associations with the secondary peak and the slope of the macular pigment spatial profile. *Invest Ophthalmol Vis Sci.* 2009;50:1383–1391.

88. Gass JDM. Müller cell cone, an overlooked part of the anatomy of the fovea centralis. *Arch Ophthalmol*. 1999;117:821–823.
89. Wang JJ, Rochtchina E, Lee AJ, et al. Ten-year incidence and progression of age-related maculopathy: the Blue Mountains Eye Study. *Ophthalmology*. 2007;114:92–98.
90. Joachim N, Mitchell P, Burlutsky G, Kifley A, Wang JJ. The incidence and progression of age-related macular degeneration over 15 years: the Blue Mountains Eye Study. *Ophthalmology*. 2015;122:2482–2489.
91. Müller S, Issa PC, Heeren TFC, Thiele S, Holz FG, Herrmann P. Macular pigment distribution as prognostic marker for disease progression in macular telangiectasia type 2. *Am J Ophthalmol*. 2018;194:163–169.
92. Delori FC, Goger DG, Hammond BR, Snodderly DM, Burns SA. Macular pigment density measured by autofluorescence spectrometry: comparison with reflectometry and heterochromatic flicker photometry. *J Opt Soc Am A Opt Image Sci Vis*. 2001;18:1212–1230.
93. Warburton S, Davis WE, Southwick K, et al. Proteomic and phototoxic characterization of melanolipofuscin: correlation to disease and model for its origin. *Mol Vis*. 2007;13:318–329.
94. Freund KB, Mrejen S, Jung J, Yannuzzi LA, Boon CJ. Increased fundus autofluorescence related to outer retinal disruption. *JAMA Ophthalmol*. 2013;131:1645–1649.
95. Edwards MM, McLeod DS, Bhutto IA, Grebe R, Duffy M, Luty GA. Subretinal glial membranes in eyes with geographic atrophy. *Invest Ophthalmol Vis Sci*. 2017;58:1352–1367.
96. Dolz-Marco R, Balaratnasingam C, Messinger JD, et al. The border of macular atrophy in age-related macular degeneration: a clinicopathologic correlation. *Am J Ophthalmol*. 2018;193:166–177.
97. Linderman RE, Muthiah MN, Omoba SB, et al. Variability of foveal avascular zone metrics derived from optical coherence tomography angiography images. *Transl Vis Sci Technol*. 2018;7:20.
98. Burgess S, Davey Smith G. Mendelian randomization implicates high-density lipoprotein cholesterol-associated mechanisms in etiology of age-related macular degeneration. *Ophthalmology*. 2017;124:1165–1174.
99. Balaratnasingam C, Chae B, Remmer MH, et al. The spatial profile of macular pigments is related to the topological characteristics of the foveal avascular zone. *Invest Ophthalmol Vis Sci*. 2015;56:7859–7865.
100. Dubis AM, Hansen BR, Cooper RF, Beringer J, Dubra A, Carroll J. Relationship between the foveal avascular zone and foveal pit morphology. *Invest Ophthalmol Vis Sci*. 2012;53:1628–1636.

## APPENDIX

Custom ImageJ plug-ins used for this research are available for download. The link to the ImageJ update site is <https://sites.imagej.net/CreativeComputation/>. Programs are available as .jar files, which include source code.

Batch_Grids_OCT	Gathers OCT data
Batch_Rezero_MPOD_OCT	Re-zeroes MPOD data
CheckFovea_OCT	Checks position of fovea and ONH
Find_Fovea_OCT	Lets user specify the location of fovea and ONH
MPOD_XML_Reader	Creates an MPOD image from MPOD XML Export
QAF_XML_Reader	Creates a QAF image from QAF XML Export
Register_OCT	Registers en face images to OCT XML Export